Implementation of phase estimation and quantum counting algorithms on an NMR quantum-information processor

Jae-Seung Lee, Jaehyun Kim, Yongwook Cheong, and Soonchil Lee
Department of Physics, Korea Advanced Institute of Science and Technology, Daejeon 305-701, Korea
(Received 6 December 2001; published 23 October 2002)

The quantum Fourier transform is a key factor in achieving exponential speedup relative to classical algorithms. We implemented the phase estimation algorithm, which is the very basic application example of the quantum Fourier transform, on a three-bit nuclear magnetic resonance quantum-information processor. The algorithm was applied to one-bit Grover operators to estimate eigenvalues. We also demonstrated the counting algorithm with the same operators to obtain the number of the marked states. The results of projective measurements required by the algorithms were obtained from the split peak positions in the spectra.

DOI: 10.1103/PhysRevA.66.042316 PACS number(s): 03.67.Lx

Quantum computation has been the subject of intense study during the last decade because quantum computers can solve certain problems that classical computers can hardly do. Much effort has been made to realize a quantum computer, but at present only the liquid state nuclear magnetic resonance (NMR) has the capability of implementing quantum algorithms. Although the liquid state NMR is believed not to be a candidate for a future practical quantum computer, the experience of implementing quantum algorithms by the NMR has been useful in understanding the basics of quantum computation and in expecting problems encountered in more scalable devices. The quantum algorithms implemented by NMR include Deutsch-Jozsa [1,2], Grover's search [3–5], order finding [6], and Shor's quantum factoring [7] algorithms.

The quantum algorithms achieving exponential speedup relative to classical algorithms have two features in common, the evaluation of a function on superposed input states and the polynomial-time quantum discrete Fourier transform (QFT) [8]. The phase estimation algorithm, which estimates eigenvalues of a unitary operator, is one of the most basic examples of such quantum algorithms and it has been studied as a way to find eigenvalues and eigenvectors of a local Hamiltonian [9–11]. In this work, we estimated the eigenvalues of one-bit Grover operators [12] by implementing the phase estimation algorithm on a three-bit NMR quantum-information processor. In a quantum search problem, the number of iterations of Grover operators necessary to find a target item depends on the number of marked states, which is reflected in the eigenvalues of those operators [13]. We also performed an experiment counting the number of marked states using the same Grover operators. In an NMR quantum-information processor, the results of projective measurements required by the original algorithm can be obtained in two ways. One way is to use the spectral implementation where computational states are assigned to individual spectral resonance lines [14] and the other way is to dephase the density operator as the projective measurement by pulsed magnetic-field gradients [15]. The former is advantageous when just numbers are required as measurement results, while the latter is effective in simulating measurement process and obtaining coherences after projective measurements. We used spectral implementation for the phase estimation algorithm since only numbers are required at the end of computation. It is even possible to read an answer with certainty from the spectrum when projective measurement can give only a probabilistic answer, theoretically.

One of the peculiar phenomena of quantum computation is that a controlled operation can change the state of a control bit. Let U be any unitary operator acting on $|y\rangle$ of dimension N and $\Gamma_M(U)$ an operator that maps $|x\rangle|y\rangle(=|x\rangle\otimes|y\rangle)$ to $|x\rangle U^x|y\rangle$, where M is the dimension of the control register $|x\rangle$. If $|\Psi\rangle$ is an eigenvector of the operator U with its eigenvalue $e^{2\pi\imath\omega}$, then $\Gamma_M(U)$ transforms the state $(1/\sqrt{M})\Sigma_{x=0}^{M-1}|x\rangle|\Psi\rangle$ to

$$\frac{1}{\sqrt{M}}\sum_{x=0}^{M-1}|x\rangle U^x|\Psi\rangle=\frac{1}{\sqrt{M}}\sum_{x=0}^{M-1}e^{2\pi\imath\omega x}|x\rangle|\Psi\rangle. \qquad (1)$$

This final state can be interpreted as meaning that the target state remains the same while the relative phase of the control register changes. Now the eigenvalue ω can be estimated by the QFT of the control register. The operator $O_{\mathrm{QFT}}(M)$ is defined on the vector space of dimension M as a transform of a state $|j\rangle$ to a state $(1/\sqrt{M})\Sigma_{x=0}^{M-1}e^{2\pi\imath(j/M)x}|x\rangle$. Application of the inverse QFT to the control register gives

$$\begin{aligned}|\omega\rangle&\equiv O_{\mathrm{QFT}}(M)^{-1}\frac{1}{\sqrt{M}}\sum_{x=0}^{M-1}e^{2\pi\imath\omega x}|x\rangle\\&=\frac{1}{M}\sum_{j=0}^{M-1}e^{\pi\imath(M-1)(\omega-j/M)}\frac{\sin[\pi(M\omega-j)]}{\sin[\pi[\omega-(j/M)]]}|j\rangle.\end{aligned} \qquad (2)$$

If $\omega=j/M$, $|\omega\rangle=|j\rangle$. Otherwise, the probability of measuring $|j\rangle$ in the final state is

$$P_{M,\omega}(j)=\left|\frac{\sin[\pi(M\omega-j)]}{M\sin[\pi[\omega-(j/M)]]}\right|^2.$$

TABLE I. One-bit Grover operators and their eigenvectors and eigenvalues.

Marked state	G	Eigenvector	Eigenvalue
None	$\begin{pmatrix} 0 & 1 \\ 1 & 0 \end{pmatrix}$	$\frac{1}{\sqrt{2}}(\|0\rangle+\|1\rangle)$	1
		$\frac{1}{\sqrt{2}}(\|0\rangle-\|1\rangle)$	-1
0	$\begin{pmatrix} 0 & 1 \\ -1 & 0 \end{pmatrix}$	$\frac{1}{\sqrt{2}}(\|0\rangle+\imath\|1\rangle)$	$\imath$
		$\frac{1}{\sqrt{2}}(\|0\rangle-\imath\|1\rangle)$	$-\imath$
1	$\begin{pmatrix} 0 & -1 \\ 1 & 0 \end{pmatrix}$	$\frac{1}{\sqrt{2}}(\|0\rangle+\imath\|1\rangle)$	$-\imath$
		$\frac{1}{\sqrt{2}}(\|0\rangle-\imath\|1\rangle)$	$\imath$
0, 1	$\begin{pmatrix} 0 & -1 \\ -1 & 0 \end{pmatrix}$	$\frac{1}{\sqrt{2}}(\|0\rangle+\|1\rangle)$	-1
		$\frac{1}{\sqrt{2}}(\|0\rangle-\|1\rangle)$	1

If the measurement result is $\bar{j}$, the eigenvalue is estimated to be $e^{2\pi\imath\bar{j}/M}$. Since $\mathrm{Prob}(|\bar{j}-M\omega|\leqslant k)\geqslant 1-[1/2(k-1)]$ for $k>1$, the correct eigenvalue is close to the estimated value with high probability.

In implementation, we used two qubits as control bits and one qubit as a target bit and chose Grover operators as the unitary operators acting on the target bit. A Grover operator G consists of an oracle and the *inversion about average* operation which is given by $-HS_0H$. Here, H is the Hadamard gate and $S_0=I-2|0\rangle\langle 0|$, where I is an identity matrix [12]. In the one qubit vector space, there are four different Grover operators corresponding to the cases where the marked state is 0, 1, both, and absent. Table I lists one-bit Grover operators and their eigenvectors with corresponding eigenvalues.

The quantum circuit for the phase estimation algorithm is shown in Fig. 1. Spin 1 is the target qubit, and spins 2 and 3

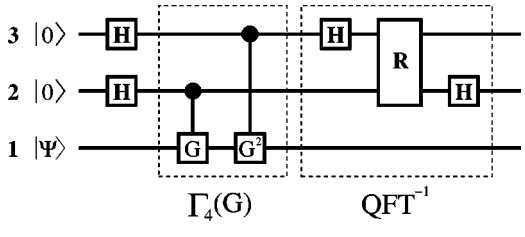

FIG. 1. The quantum circuit for the phase estimation algorithm. The numbers at the left side are the indices of carbon spins. The spins 2 and 3 are initialized to the state $|0\rangle|0\rangle$ and the spin 1 to one of the two eigenstates of a one-bit Grover operator G. H and R are the Hadamard and conditional phase gates, respectively.

TABLE II. Parameters for pulse sequences of $\Gamma_4(G)$.

Marked state	ϕ	α	β	γ
None	y	$-\frac{\pi}{2}$	$-\frac{\pi}{2}$	0
0	x	$-\frac{\pi}{2}$	0	π
1	x	$-\frac{\pi}{2}$	π	π
0, 1	y	$-\frac{\pi}{2}$	$\frac{\pi}{2}$	0

are the control qubits. In the first stage, $\Gamma_4(G)$ consists of controlled-G and controlled-G^2 operations. The controlled-G operations were decomposed by using the method in Ref. [16] to get the NMR pulse sequence in temporal order,

$$I_{1\phi}\left(-\frac{\pi}{2}\right)-I_{1z}(\alpha)-I_{2z}(\beta)-J_{12}\left(\frac{\pi}{2}\right)-I_{1\phi}\left(\frac{\pi}{2}\right), \quad (3)$$

where the subscripts indicate the indices of spins and the axes of rotations. A pulse $I_{j\phi}(\theta)$ is given by $\exp[-\imath(\theta/2)\sigma_{j\phi}]$, where $j=1,2$, $\phi=x,y,z$, and $J_{12}(\theta)=\exp[-\imath(\theta/2)\sigma_{1z}\sigma_{2z}]$. Since G^2's are proportional to $\pm I$, the controlled-G^2 operation can be realized by a single rotation $I_{3z}(\gamma)$. Table II summarizes the parameters ϕ, α, β, and γ for four different $\Gamma_4(G)$'s. In the second stage, the inverse QFT [17] is decomposed into two Hadamard gates and a conditional phase gate $R=\mathrm{diag}[1,1,1,e^{-\imath(\pi/2)}]$. The Hadamard gate on the jth qubit, H_j, can be realized by either $I_{jy}(-\pi/2)-I_{jz}(\pi)$ or $I_{jz}(\pi)-I_{jy}(\pi/2)$. We chose $I_{3y}(-\pi/2)-I_{3z}(\pi)$ for H_3 and $I_{2z}(\pi)-I_{2y}(\pi/2)$ for H_2 to simplify the total pulse sequence. The conditional phase gate R is decomposed into

$$I_{2z}\left(-\frac{\pi}{4}\right)-I_{3z}\left(-\frac{\pi}{4}\right)-J_{23}\left(\frac{\pi}{4}\right) \quad (4)$$

by using the same method as the controlled-G operation. Therefore, the pulse sequence for the inverse QFT is given by

$$I_{3y}\left(-\frac{\pi}{2}\right)-I_{3z}\left(\frac{3}{4}\pi\right)-I_{2z}\left(\frac{3}{4}\pi\right)-J_{23}\left(\frac{\pi}{4}\right)-I_{2y}\left(\frac{\pi}{2}\right). \quad (5)$$

Since this implementation of the inverse QFT swaps the output states of spins 2 and 3, the least significant digit of the control register at input becomes the most significant one at output. The algorithm requires eigenvectors of U as input [see Eq. (1)]. The eigenvectors of the one-bit Grover operators are equally weighted superpositions of $|0\rangle$ and $|1\rangle$ states (Table I). Therefore, each state can be prepared by a single 90° pulse. In experiments, this single pulse and the following first pulse of the controlled-G operation are canceled or added to a single 180° pulse. At the end of the pulse sequence, the original algorithm requires the measuring of the state of the control register, which consists of spins 2 and 3.

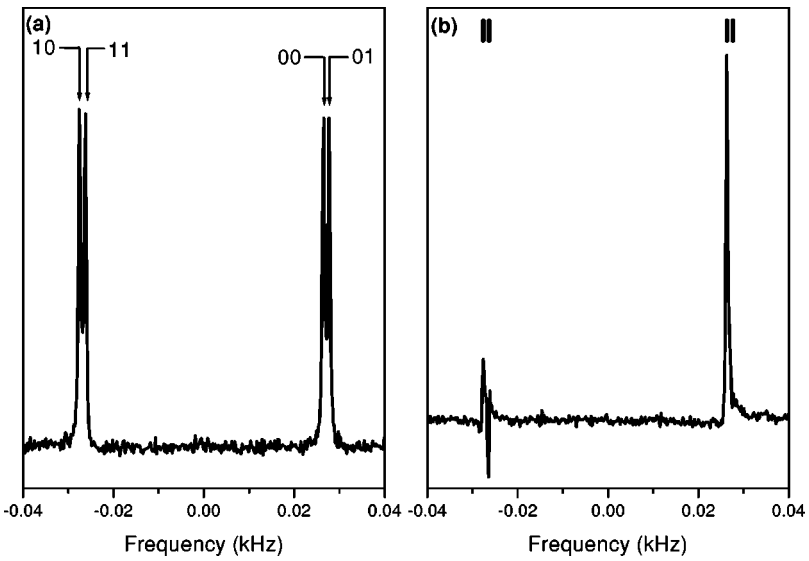

FIG. 2. (a) The spectrum of the spin 1 when the spins are in thermal equilibrium. Four split peaks are observed due to spin-spin couplings J_{12} and J_{13}. The labels of the peaks represent the states of the control register. The most and least significant bits represent the state of the spins 2 and 3, respectively. (b) The same spectrum when the spins are in the effective pure state $|0\rangle|0\rangle|0\rangle$. Only the absorptive and positive peak labeled 00 is present, as expected.

Instead, the spectrum of the spin 1 is used to get information on the states of the spins 2 and 3 as explained later.

As the qubits, three ^{13}C nuclear spins of 99% carbon-13 labeled alanine [$C^1O_2^-$-$C^2H(C^3H_3)$-NH_3^+] in D_2O solvent were used. With proton decoupling, the dynamics of three carbon spins are described by the Hamiltonian

$$\mathcal{H}=\omega_1 I_{1z}+\omega_2 I_{2z}+\omega_3 I_{3z}+\pi J_{12} 2I_{1z}I_{2z}+\pi J_{13} 2I_{1z}I_{3z} + \pi J_{23} 2I_{2z}I_{3z}, \quad (6)$$

where $I_i=\sigma_i/2$ are rescaled Pauli matrices and J_{ij} are scalar coupling constants. The experiments were carried out on a Bruker DRX300 spectrometer with the resonance frequency of 75.475 MHz. The chemical shifts of three carbon spins relative to the carrier frequency are about 6019.8, -3437.4, and -6032.2 Hz, and the coupling constants J_{12}, J_{23}, and J_{13} are 54.06, 34.86, and -1.3 Hz, respectively. On-resonance excitations of three carbon spins were achieved by phase-ramping techniques [18]. All pulses were spin selective and the duration of the pulses was about 2 ms. UBURP (universal 90° band-selective, uniform response, pure-phase) and REBURP (refocusing 180° BURP) pulses [19] were used for 90° and 180° single-qubit rotations, respectively. By adjusting the phases of the subsequent pulses, rotations about the z axis were implemented and the transient Bloch-Siegert effects [20] were compensated for. No phase cycling was used in all experiments.

An effective pure initial state was obtained by temporal averaging [21] in a way introduced in Ref. [6]. For a homonuclear three-spin system, the deviation density matrix of the thermal equilibrium state is the sum of three product operators: $\rho_{th}=I_{1z}+I_{2z}+I_{3z}$. From this mixed density matrix, four density matrices, $\rho_1=2I_{1z}I_{3z}+I_{2z}+I_{3z}$, $\rho_2=-2I_{1z}I_{2z}+I_{2z}+I_{3z}$, $\rho_3=I_{1z}-2I_{2z}I_{3z}+I_{3z}$, and $\rho_4=I_{1z}+4I_{1z}I_{2z}I_{3z}+I_{3z}$, were created by short pulse sequences. The deviation density matrix of the effective pure state $|000\rangle$ can be obtained by $\rho_{th}+\rho_1-\rho_2-\rho_3+\rho_4$. Figure 2 shows the spectrum of spin 1 when the spins are in the thermal equilibrium state (a) and that after temporal averaging (b). When reading a spectrum, a positive absorptive peak is interpreted to represent the $|0\rangle$ state and a negative $|1\rangle$ state. In thermal equilibrium, four split peaks are observed due to the spin-spin couplings with spins 2 and 3. The four peaks in Fig. 2(a) represent $|000\rangle$, $|001\rangle$, $|010\rangle$, and $|011\rangle$ states. This means that we can read the final state of the control register in the spectrum of the target register. In spectrum (b), all the peaks disappear except the one corresponding to $|000\rangle$, as expected.

We performed eight experiments with four different Grover operators and two eigenvectors as input states for each operator. Figure 3 shows the spectra of the spin 1 acquired after the execution of the algorithm. The intensity ratios of the final signal to the initial one, which is a measure of precision in implementation, is about 60–80 % depending on experiment time. In all cases, only one of the four split lines is observed, meaning that the control register is not in a superposed state, that is, these are the cases when $\omega=j/M$. Therefore, the state of the control register, $|\vec{j}\rangle$, is clearly determined and from it, the eigenvalue is estimated as $\exp[2\pi\imath(\vec{j}/4)]$. For example, the spectrum in Fig. 3(a2) shows a peak corresponding to the $|010\rangle$ state giving a control register value of 2. Therefore, the eigenvalue is $\exp[2\pi\imath(2/4)]=-1$, as expected from the second eigenstate of the Grover operator for the case of no marked state in Table I. It is easy to check whether the other spectra also give correct eigenvalues.

The eigenvalues of a Grover operator contain information on the number of marked states in a search problem. In fact, the algorithm counting the number of marked states differs from the phase estimation of a Grover operator only in the initial state preparation of the target register [13]. The same phase estimation procedure enables us to count the number of the marked states t if the target state is initially set to be $(1/\sqrt{2})(|0\rangle+|1\rangle)$. This state can be expressed as $(e^{\pi\imath\omega}/\sqrt{2})|\Psi_+\rangle+(e^{-\pi\imath\omega}/\sqrt{2})|\Psi_-\rangle$ using the eigenvectors $|\Psi_\pm\rangle$ as bases. After the execution of the algorithm, the state becomes

$$\frac{e^{\pi\imath\omega}}{\sqrt{2}}|\omega\rangle|\Psi_+\rangle+\frac{e^{-\pi\imath\omega}}{\sqrt{2}}|-\omega\rangle|\Psi_-\rangle, \quad (7)$$

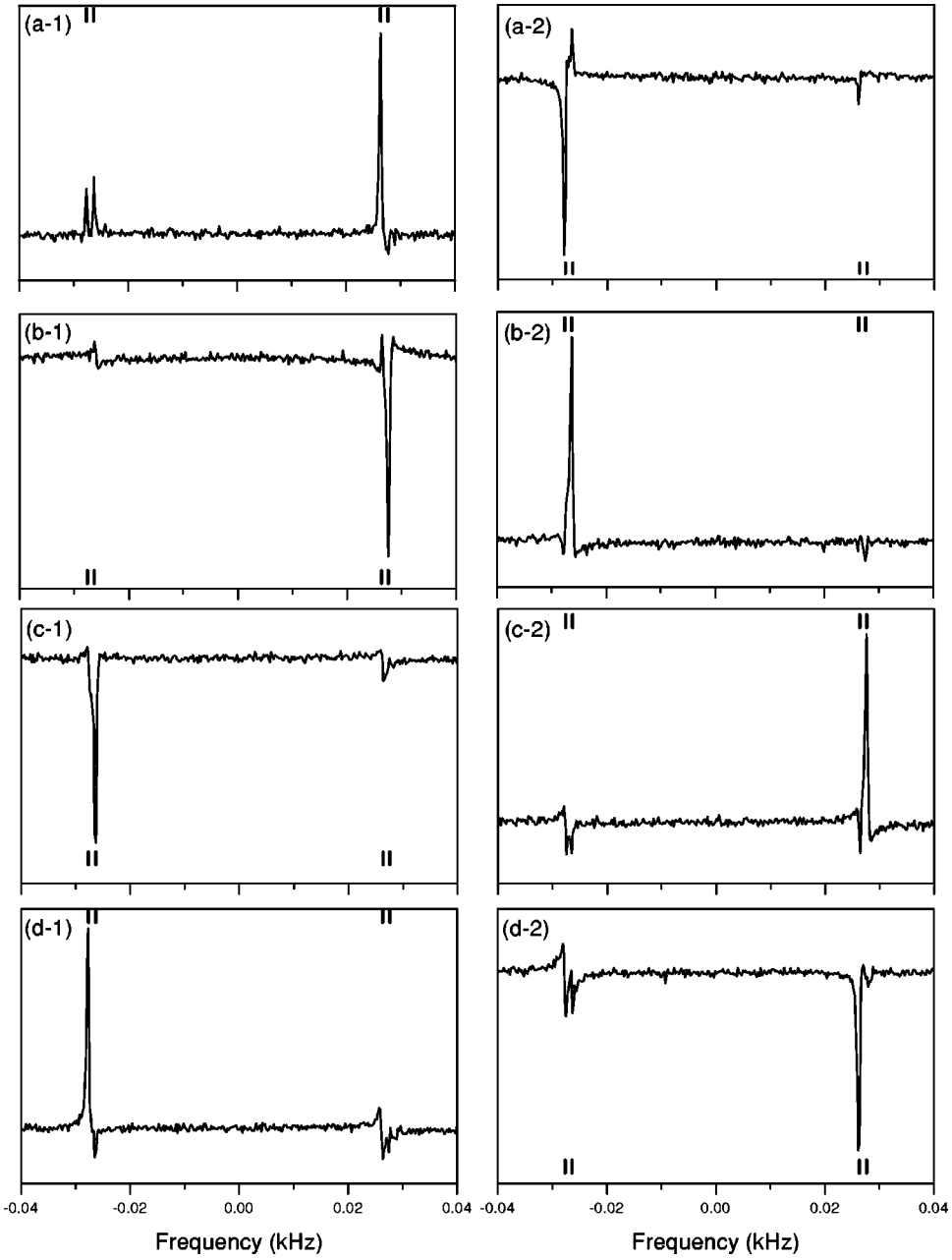

FIG. 3. Spectra of the spin 1 after the execution of the phase estimation algorithm. The positions of four peaks in the spectrum of the thermal equilibrium state are indicated with short bars. (a) ''No marked state'' case: the input states are $(1/\sqrt{2})(|0\rangle+|1\rangle)$ for (a1) and $(1/\sqrt{2})(|0\rangle-|1\rangle)$ for (a2). These states remain same through the experiment and appear in the spectrum as positive and negative peaks, respectively. The peak positions represent that the states of the control register are 0 for (a1) and 2 for (a2). (b) ''Marked state 0'' case: the states of the control register are 1 for (b1) and 3 for (b2). (c) ''Marked state 1'' case: the states of the control register are 3 for (c1) and 1 for (c2). (d) ''All marked states'' case: the states of the control register are 2 for (d1) and 0 for (d2).

where $|\omega\rangle$ is defined in Eq. (2). If a projective measurement on the control register gives some number $\overline{j}$, it should be close to $M\omega$ or $M(1-\omega)$ with high probability. Then t is estimated to be $2\sin^2(\pi\overline{j}/M)$, which is independent of the sign of the measured value $\overline{j}$.

Figure 4 shows the spectra of spin 1 after the execution of the counting algorithm when the marked state is 0 (a) and 1 (b). Each spectrum looks like a superposition of two spectra in Fig. 3 that were obtained with the initial target state consisting of only one eigenvector. The control register is in the mixture of $|01\rangle$ and $|11\rangle$ states in both spectra, giving 1 or 3 as possible measurement values. From these values, we get $t=2\sin^2(\pi/4)=2\sin^2(3/4\pi)=1$. In the ''no marked state'' and ''all marked states'' cases, the results are the same as those of the phase estimation experiments since the initial superposed target state in the counting algorithm happens to be the eigenvector of the corresponding Grover operators. Therefore, the result of counting can be read from Figs. 3(a1) and (d1) that give $t=0$ and 2, respectively. The same results have been obtained by Jones and Mosca [22] in a different way, in which t is estimated by modulating signal intensities of the one qubit control register with successive applications of the controlled-G operation.

In our experiments, the results expected after the projective measurement of the control register were read from the spectrum of the target register. Only one of the four split lines was observed in the phase estimation of a Grover operator because the final state of the control register is not superposed. If the eigenvalue of some operator other than Grover operators is unequal to j/M, however, the control register is in the superposed final state and the algorithm gives an eigenvalue that is close to the correct value with

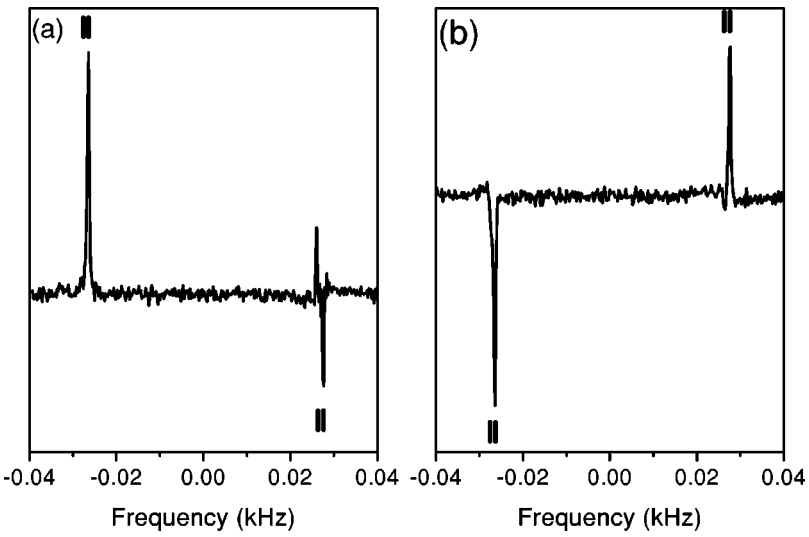

FIG. 4. Results of the quantum counting algorithm. The input state is $(1/\sqrt{2})(|0\rangle+|1\rangle)$. (a) ''Marked state 0'' case: the spectrum looks like the superposition of spectra Figs. 3(b1) and (b2). (b) ''Marked state 1'' case: the spectrum looks like the superposition of spectra Figs. 3(c1) and (c2). Asymmetry in peaks is caused by imperfect pulses.

high probability. In this case, several peaks are expected in the NMR spectrum and the label of the highest peak gives the same value as the projective measurement because the area of each peak in the spectrum is proportional to $P_{M,\omega}(j)$. This also indicates that the result of a calculation in an ensemble quantum computer can be obtained from the knowledge of a part of the density matrix of the output state rather than the full matrix. The algorithms using the QFT such as the phase estimation or a period-finding problem [23] belong to this case.

In the case of the counting experiment, the areas are proportional to $P_{M,\omega}(j)-P_{M,-\omega}(j)$, where $P_{M,\omega}(j)$ and $P_{M,-\omega}(j)$ are the probabilities of measuring j in $|\omega\rangle$ and $|-\omega\rangle$ states, respectively. This is because the spectrum contains both of the orthogonal target states $|\Psi_{\pm}\rangle$, whose phases are opposite to each other. In spite of this averaging effect, there is practically no problem in estimating t because $P_{M,\pm\omega}(j)$ decay so fast from their peak positions that their values are ignorable at each other's peak positions.

In summary, phase estimation and counting algorithms were demonstrated for one-bit Grover operators on a three-bit NMR quantum-information processor. The final state of the control register was read from the spectrum of the target register. The label of the highest peak gives the same answer as the projective measurement of the control register.

We thank the Korea Basic Science Institute for use of the spectrometer. This work was partially supported by the BK21 Project, NRL Program, and KOSEF via eSSC at POSTECH.

[1] J.A. Jones and M. Mosca, J. Chem. Phys. **109**, 1648 (1998).
[2] I.L. Chuang, L.M.K. Vandersypen, X. Zhou, D.W. Leung, and S. Lloyd, Nature (London) **393**, 143 (1998).
[3] I.L. Chuang, N. Gershenfeld, and M. Kubinec, Phys. Rev. Lett. **80**, 3408 (1998).
[4] J.A. Jones, M. Mosca, and R.H. Hansen, Nature (London) **393**, 344 (1998).
[5] L.M.K. Vandersypen, M. Steffen, M.H. Sherwood, C.S. Yannoni, G. Breyta, and I.L. Chuang, Appl. Phys. Lett. **76**, 646 (2000).
[6] L.M.K. Vandersypen, M. Steffen, G. Breyta, C.S. Yannoni, R. Cleve, and I.L. Chuang, Phys. Rev. Lett. **85**, 5452 (2000).
[7] L.M.K. Vandersypen, M. Steffen, G. Breyta, C.S. Yannoni, M.H. Sherwood, and I.L. Chuang, Nature (London) **414**, 883 (2001).
[8] D. Coppersmith, IBM Research Report No. RC19642, 1994 (unpublished).
[9] D.S. Abrams and S.L. Lloyd, Phys. Rev. Lett. **83**, 5162 (1999).
[10] B.C. Travaglione and G.J. Milburn, Phys. Rev. A **63**, 032301 (2001).
[11] M. Hillery and V. Bŭzek, Phys. Rev. A **64**, 042303 (2001).
[12] L.K. Grover, Phys. Rev. Lett. **79**, 325 (1997).
[13] G. Brassard, P. Høyer, M. Mosca, and A. Tapp, e-print arXiv:quant-ph/0005055.
[14] Z.L. Mádi, R. Brüschweiler, and R.R. Ernst, J. Chem. Phys. **109**, 10 603 (1998).
[15] G. Teklemariam, E.M. Fortunato, M.A. Pravia, T.F. Havel, and D.G. Cory, Phys. Rev. Lett. **86**, 5845 (2001).
[16] J. Kim, J.-S. Lee, and S. Lee, Phys. Rev. A **61**, 032312 (2000).
[17] The QFT has been implemented on three qubits, see Phys. Rev. Lett. **86**, 1889 (2001) and Refs. [6,7].
[18] J. Boyd and N. Soffe, J. Magn. Reson. **85**, 406 (1989).
[19] H. Geen and R. Freeman, J. Magn. Reson. **93**, 93 (1991).
[20] L. Emsley and G. Bodenhausen, Chem. Phys. Lett. **168**, 297 (1990).
[21] E. Knill, I.L. Chuang, and R. Laflamme, Phys. Rev. A **57**, 3348 (1998).
[22] J.A. Jones and M. Mosca, Phys. Rev. Lett. **83**, 1050 (1999).
[23] M. A. Nielsen and I. L. Chuang, *Quantum Computation and Quantum Information* (Cambridge University Press, Cambridge, 2000).